# Highly selective electroplated nickel mask for lithium niobate dry etching

Sarah Benchabane,[a] Laurent Robert, Jean-Yves Rauch, Abdelkrim Khelif, and Vincent Laude
*Institut FEMTO-ST, Université de Franche-Comté, CNRS, ENSMM, UTBM, 32 Avenue de l'Observatoire, F-25044 Besançon Cedex, France*

(Received 25 November 2008; accepted 29 March 2009; published online 11 May 2009)

A sulfur hexafluoride based reactive ion etching process allowing to etch several micron deep holes with diameters of the order of a few microns in lithium niobate is reported. Etching of deep structures with aspect ratios up to 1.5 was made possible through the use of an electroplated nickel mask exhibiting a selectivity as high as 20 with respect to lithium niobate. Several crystallograpic orientations were investigated, although particular interest was paid to *Y*-axis oriented substrates. Photoresist as well as metal masks were also tested and their selectivity was compared. The influence of process parameters such as applied rf power or operating pressure on the sidewall slope angle of the etched patterns was investigated. The technique has been successfully applied to the fabrication of phononic crystals consisting of periodical arrays of 9 $\mu$m diameter, 10 $\mu$m deep holes, with a 10 $\mu$m period, and presenting sidewall angles as high as 73° etched in *Y*-axis oriented lithium niobate. © *2009 American Institute of Physics*. [DOI: 10.1063/1.3125315]

## I. INTRODUCTION

The remarkable physical properties of lithium niobate make this material a key element in a number of applications pertaining to integrated optoelectronics or high frequency acoustics. Its high nonlinear, electro-optical or acousto-optical coefficients, its piezoelectric properties, or the possibilities it offers in terms of waveguide fabrication allow for the realization of both active and passive devices. A significant effort has been devoted to etch this material to widen its application range or just to take full advantage of its intrinsic capabilities. Ridge waveguides for electro-optical modulators[1] or much more recently photonic crystals[2] are typical examples of structures to be efficiently achieved. Yet, however well known and widely used lithium niobate might be, it still remains a nonconventional material from a microfabrication point of view: processes for fabrication of fine features with high aspect ratios are not readily available. Instead, a variety of wet and dry etching techniques have been investigated for several decades without leading to a clear and well-defined process. Wet etching, for example, is generally realized using a fluorhydric acid-based mixture.[3] It predominantly relies on the material ferroelectric properties and on the difference in etch rates between positive and negative *Z* faces in lithium niobate. It hence remains limited to substrates with a *Z*-axis crystallographic orientation on which electric field poling is preliminarily applied. This method is far from being devoid of interest as depths of several tenths of microns can be reached.[4] Differential etching through domain inversion, however, highly depends on the initial crystal quality and can result in significant roughness if the material is not fully single domain. An alternative consists in using techniques such as proton exchange to alter the material properties prior to wet etching, which presents the advantage of its possible implementation on *X*-axis oriented substrates as well.[5] Still, proton-exchange-based techniques limit the achievable depth over a single run to the exchanged depth which rarely exceeds a couple of microns. Eventually, these two processes are highly sensitive to the crystallographic orientation and are not applicable to *Y*- and *Y*-rotated crystallographic faces of lithium niobate which are of significant interest in the field of acoustics.

Dry etching, conversely, can be applied to any crystallographic orientation, with or without preliminary alteration of the material. If the idea of dry etching lithium niobate with ion-beam milling has emerged in the mid-1970s,[6,7] works dedicated to the field remain quite numerous. Focused ion-beam milling has been successfully applied to the fabrication of submicron structures,[8,9] but remains time consuming and difficult to implement when dealing with large patterns or at wafer level. Alternative techniques such as femtosecond or UV laser ablation[10–12] or more recently neutral loop discharge[13] have also been introduced. However, reactive ion etching (RIE) and inductively coupled plasma-RIE (ICP-RIE) remain among the most interesting and accessible methods. RIE is in itself a highly controllable and versatile dry process involving both physical and chemical effects to achieve directive and anisotropic material removal. It has already been demonstrated that lithium niobate can be dry etched using fluorine-based chemistries,[14–17] and ICP-RIE has previously been used on *X*- or *Z*-axis crystallographic orientations of lithium niobate to successfully fabricate ridge waveguides or photonic crystals, usually after proton exchange[18–20] but there is no report of any specific process allowing to dry etch structures that are several microns in depth in lithium niobate. The fabrication of very deep or very high aspect ratio structures is actually seriously impaired by the formation of lithium fluoride (LiF) compounds during the etching process that are relatively nonvolatile, leading to redeposition phenomena impeding the material removal.[21] Most of the previous works related to RIE or ICP-RIE have

[a]Author to whom correspondence should be addressed. Electronic mail: sarah.benchabane@femto-st.fr.

 

reported hole depths less than 5 $\mu$m, the attainable depth usually being limited by the mask selectivity, that is, by the ratio of the etch rate of the mask to the etch rate of the substrate. Reported mask selectivities usually lie below 10:1. This value is high enough for the fabrication of ridge waveguides or photonic crystals provided that the mask can be made thick enough given the high resolution needed and that the side wall slope angle remains vertical enough. The reported processes, however, cannot be used for the fabrication of microsonic phononic crystals for surface acoustic waves, where lattice parameters are of several microns and where the required diameter over pitch ratio can be as high as 90%,[22] generating the need for several micron deep holes while maintaining a high resolution. This last condition, along with the need to work on *Y*- or *Y*-rotated crystallographic faces, calls for the use of dry etching. Because of the required etched depth, the mask selectivity appears like the key issue in the process to be developed.

In this work, we report on a RIE-based technique for etching a few micron-sized holes which are several microns in depth, with aspect ratios larger than 1.5, using an electroplated nickel mask exhibiting a selectivity of 20. The process has been developed in a standard RIE machine. Several crystal orientations have been investigated, although particular interest has been devoted to *Y*-crystallographic orientation of lithium niobate. Pattern sizes in the 5–15 $\mu$m range were aimed at with aspect ratios exceeding 1, meaning that the obtaining of hole depths larger than 10 $\mu$m was intended for. The technique is evaluated through the fabrication of square lattice phononic crystals consisting of periodical arrays of 9 $\mu$m diameter, 10 $\mu$m deep holes, with a 10 $\mu$m period.

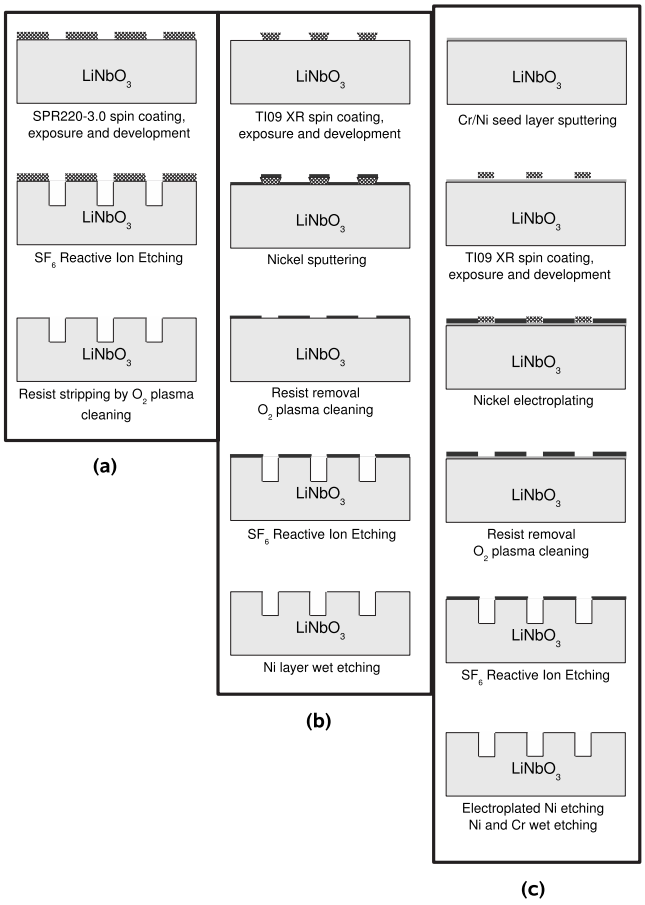


FIG. 1. Process steps for the realization of the three etching masks used. (a) Photoresist mask, (b) sputtered Ni mask, and (c) electroplated Ni mask.

## II. MASK SELECTIVITY

Test patterns consisting of arrays of octogons with diameters varying from 1.2 to 16 $\mu$m have been used to assess first the mask selectivity, then the RIE process itself on *Y*-axis oriented $LiNbO_3$ samples. The etching has been performed in a standard RIE machine (Plassys MG 200) allowing for a maximum rf power of 250 W. The process is based on a sulfur hexafluoride ($SF_6$) chemistry at relatively low pressure (between 0.15 and 0.2 Pa) with an applied rf power equal to 150 W and a gas flow of 10 SCCM (SCCM denotes cubic centimeter per minute at STP), giving a bias (or autopolarization) voltage around 650 V and resulting in a $LiNbO_3$ etch rate around 40 nm $min^{-1}$. Three different etching masks have been investigated: a plasma-resistant photoresist (Megaposit SPR-220 3.0, commercialized by Rohm and Haas), a sputtered nickel layer, and an electroplated nickel layer. The corresponding process steps are outlined in Fig. 1. The plasma-resistant photoresist was directly patterned through UV lithography. The processes resulting in the definition of the two metal masks make use of an image reversal photoresist (MicroChemicals TI 09XR) patterned with different exposure energies to obtain either a negative wall profile to allow for a lift-off process in the sputtered Ni case or vertical sidewalls for Ni electroplating. The results obtained for each run are reported in Table I.

The 3.3 $\mu$m thick plasma-resistant photoresist film could only survive 30 min in the highly energetic $SF_6$ plasma, limiting the attainable depth to 1.2 $\mu$m. Thermal degradation of the photoresist also occurred, as could be deduced from the resilience to stripping of the residual resist layer. A 10 min long oxygen plasma cleaning was actually necessary to remove it. The SPR220 selectivity is hence pretty low (equal to 0.4) and tests performed with other thin resists based on Novolak resin did not prove any more conclusive.

Metal masks thus appeared like a more promising alternative. Preliminary tests have shown that sputtered chromium or nickel thin films exhibit a selectivity of the order of 10:1 with respect to lithium niobate. A relatively thick de-

TABLE I. Etching parameters and characteristics of *Y*-axis oriented lithium niobate for different etching masks. In all cases, the operating pressure is 0.2 Pa and the applied rf power is 150 W. The corresponding etch rate for lithium niobate is 40 nm $min^{-1}$.

| Mask | Thickness ($\mu$m) | Selectivity | Maximum hole depth ($\mu$m) |
|---|---|---|---|
| SPR220–3.0 | 3.3 | 0.4:1 | 1.2 |
| Sputtered Ni | 0.8 | 10:1 | 6 |
| Electroplated Ni | 1.0 | 16:1 | 16 |

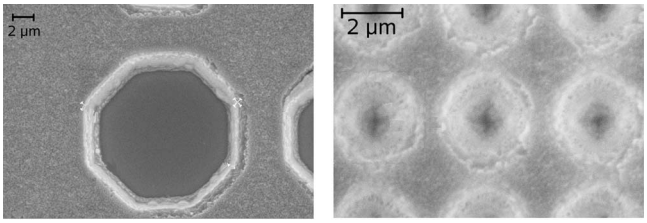


FIG. 2. SEM photographs of etched lithium niobate using a sputtered nickel layer as the etching mask. The diameters of the holes are 14 $\mu$m in (a) and 3 $\mu$m in (b). The etching parameters are as follows: rf power: 150 W; operating pressure: 0.2 Pa.

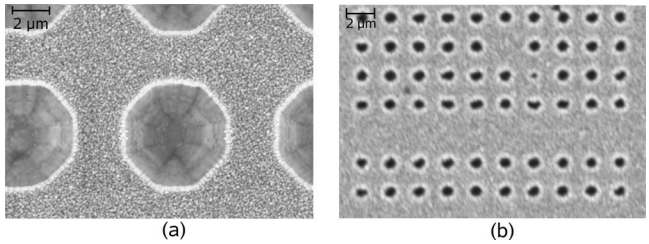


FIG. 3. SEM photographs of etched lithium niobate using an electroplated nickel layer as the etching mask. The diameters of the holes are 6 $\mu$m in (a) and 1 $\mu$m in (b). The etching parameters are as follows: rf power: 150 W; operating pressure: 0.2 Pa.

posited metal layer is then needed to etch several micron deep holes. The layer thickness, however, is limited not only by sputtering (or evaporation) as a deposition method *per se*, which does not allow for deposition of several micron thick films, but also by the photoresist used to perform the lift-off process. It is indeed necessary to allow for a large enough difference between the photoresist thickness and the deposited metal thickness to be able to achieve a lift-off process: the coated resist layer must remain significantly thicker than the deposited metal layer. In our case, we chose to use a 1.2 $\mu$m thick image reversal photoresist since a resolution of the order of 1 $\mu$m was aimed at.

The sputtered metal layer thickness was thus set to 800 nm to comply with the mentioned technological constraints. In any case, sputtering does not allow for deposition of much thicker layers without overheating the substrate. This is prohibitive in the case of lithium niobate that is highly pyroelectric. Scanning electron microscope (SEM) images of one of the etched samples are displayed in Fig. 2. In particular, holes with diameters of 14 and 3 $\mu$m are represented. In both cases, the hole depth is about 6 $\mu$m for a sidewall slope angle of 65°. This wall profile is partly due to the process itself, and partly linked to a transfer of the initial sidewall slope of the lifted-off layer constituting the metal mask. The main issue encountered here lies in the pattern edge definition, as can be seen on the SEM images. Figure 2 shows that bulges formed around the etched holes, which was confirmed by surface profile measurements realized using standard profilometry. This has neither been observed when using a photoresist as the etching mask nor in the case of electroplated nickel as will be shown later. We hence believe that this phenomenon is due to a redeposition of the sputtered material around the edge of the holes. The redeposited metal would induce some micromasking of the edges of the holes, locally preventing etching of the lithium niobate substrate and resulting in such a poor pattern edge definition. This edge effect is definitely prohibitive in the case of small diameters. Figure 2(b) shows that 3 $\mu$m diameter holes are wholly obstructed, completely preventing $LiNbO_3$ etching to occur. Edge definition of larger patterns, like the 14 $\mu$m diameter hole of Fig. 2(a), is also most unsatisfactory. In addition, as the etching process goes along, the sputtered Ni layer obviously gets thinner and thinner and the process duration required for etching hole depths of the order of 10 $\mu$m generally leads to an almost total depletion of the metallic mask. The thin metal film porosity then results in local and nonuniform etching of the lithium niobate substrate hence inducing a deterioration of the overall surface state. As far as the selectivity is concerned, the measured value (around 10) is comparable to the maximum selectivity that has been reported in the literature for sputtered or evaporated metal masks with respect to pure lithium niobate (see, e.g., Refs. 18 and 19). This basically means that the etch depth is limited to values below 8 $\mu$m given the maximum Ni thickness that can be deposited. This limit, combined with the limited mask thickness and the poor pattern edge definition, hence makes it necessary to look for alternative materials.

A solution can then consist in using thicker masks or layers with a different growth morphology. Electroplated nickel is particularly well suited to fulfill these requirements: not only can it be grown as several micron thick films but it also exhibits mechanical properties that differ quite significantly from those of its sputtered or evaporated equivalents. The electroplating process can be very briefly described as follows: a metal layer is grown onto a thin conductive layer through a galvanic process performed in a suitable electrolyte bath (here, nickel sulfamate at 50 °C). The growth can be made selective by insulating parts of the substrate with a photoresist, for instance. Electroplating hence allows for a good control of the metal wall profile as this latter directly depends on the photoresist profile used as an insulator. The electroplated metal thickness must then remain lower than the resist thickness to keep the patterns as defined by the lithography process: once again, the targeted resolution is going to limit the maximum electroplated Ni thickness. The process implemented is shown in Fig. 1(c). A seed layer made of a 40 nm thick layer of nickel, sputtered atop a 10 nm chromium layer, was first deposited. A negative photoresist layer was then spin coated, exposed, and developed with suitable conditions to achieve a 1.2 $\mu$m thick film with a vertical wall profile. A 1 $\mu$m thick Ni layer was then electroplated at a current density of 1.5 A $dm^{-1}$ (deposition rate around 13 $\mu m\ h^{-1}$) before removal of the photoresist using an acetone bath and oxygen-plasma cleaning. We chose not to remove the seed layer prior to the $LiNbO_3$ etching process: removing it through wet etching can affect the pattern size and alter the electroplated Ni surface.

The substrate was then etched using the previously mentioned RIE parameters for 3 h, knowing that the first 10 min of the process was devoted to etch the seed layer. Holes with diameter larger than 5 $\mu$m showed a depth of 6.5 $\mu$m, as illustrated in Fig. 3(a) which features holes etched in Y-cut

TABLE II. Selectivity of electroplated nickel over lithium niobate and lithium niobate etch rate for selected process parameters.

| rf power (W) | Pressure (Pa) | Selectivity | Etch rate (nm min$^{-1}$) |
|---|---|---|---|
| 150 | 0.2 | 16:1 | 40 |
| 200 | 0.2 | 20:1 | 50 |
| 200 | 0.9 | ··· | 36 |
| 200 | 6 | 10:1 | 20 |

lithium niobate before removal of the electroplated Ni mask. The thickness of the remaining mask was high enough to be evaluated even through SEM observation as can be seen in Fig. 3 and was afterwards measured with a profilometer to be around 600 nm, meaning that the mask selectivity with respect to lithium niobate was around 16. The sidewall slope angle was evaluated to be around 68° through SEM imaging by taking several images at different tilt angles and applying basic trigonometrical formulas. Patterns with diameter of 1 $\mu$m could as well be defined, as shown in Fig. 3(b), which is a definite improvement when compared to sputtered Ni masks patterned through UV lithography, although the etched depth has not been measured in this particular case. The electroplated Ni and the remaining seed layers can be etched successively using appropriate etchants. This last mask was then chosen as a basis for the RIE process development.

## III. INFLUENCE OF THE ETCHING PARAMETERS

The working pressure and the rf power were then modified to evaluate the influence of these two parameters on the etch rate, mask selectivity, and sidewall slope angle.

The pressure was first maintained at 0.2 Pa and the rf power was varied from 100 to 250 W with 50 W steps. Table II reports on the measured process characteristics. It can be seen, in particular, that the etch rate increases slightly with the applied power and is measured to be around 50 nm min$^{-1}$ at 200 W versus 40 nm min$^{-1}$ at 150 W. The selectivity is also affected, as it rises up to 20:1 at 200 W against 16:1 at 150 W. The most relevant result, however, lies in the evolution of the side wall slope angle with the rf power, which is reported in Fig. 4. This angle was measured for holes with diameters around 6, 10, and 14 $\mu$m, respectively. The first observable trend is that the sidewall verticality increases with increasing power, reaching 73° at 200 W and 79° at 250 W. The second one is that, for the same operating pressure and power, the sidewall slope angle decreases with decreasing aperture size as can be seen again in Fig. 4. This is clearly a limitation of this RIE process as it shows that the realization of micron or submicron-sized cylindrical patterns will be strongly impeded, as the sidewalls may join before a reasonable hole depth can be reached. SEM images of structures with a 6 $\mu$m diameter etched at rf powers of 200 and 250 W are displayed in Fig. 5. In both cases, the images were taken straight after etching, before removal of the etching mask. The improvement of the sidewall slope angle with the applied rf power is obvious, as can be seen in Fig. 5(a) showing the result obtained at 250 W, but

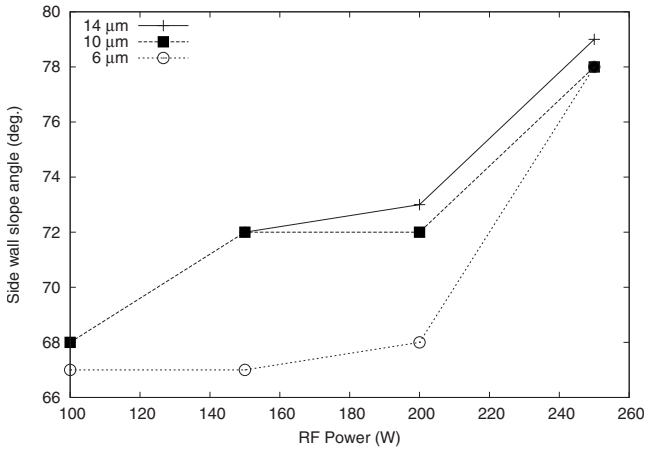


FIG. 4. Evolution of the sidewall slope angle as a function of applied rf power. The pressure was kept at a constant value of 0.2 Pa.

this, however, happens at the expense of the surface state of both the substrate surface and the bottom of the etched holes. The surface of the sample etched at 200 W remains as smooth as the initial $LiNbO_3$ surface as it was checked by surface roughness profilometric measurements.

The operating rf power was thus set to 200 W to set a trade-off between slope angle and etching quality. The pressure was then increased from 0.2 Pa, which is the minimum pressure value at which we could operate, to 0.9 and 6 Pa. Here again, the influence of this parameter on etch rate and electroplated mask selectivity is reported in Table II. The first observed consequence is that the higher the pressure is, the lower the etch rate, as the latter is around 36 nm min$^{-1}$ at 0.9 Pa and below 20 nm min$^{-1}$ at 6 Pa. The main issue, however, lies in the decrease in Ni electroplated selectivity with respect to lithium niobate with increasing pressure. This parameter is reduced by a factor over 2 at 6 Pa, ending up being equal to 10 only. Figure 6(b) shows in addition that the electroplated nickel mask is significantly altered: the Ni surface is much smoother than before etching or after etching at lower pressure values and the mask edges are strongly attacked, resulting in a gradual retractation of the etching mask and leading to a loss in the pattern edge resolution. A slight decrease in the sidewall verticality was also observed, as the angle was found to be around 68° at 6 Pa.

## IV. DISCUSSION AND APPLICATIONS

In the light of the presented results, it hence appears, quite unsurprisingly, as this observation agrees well with

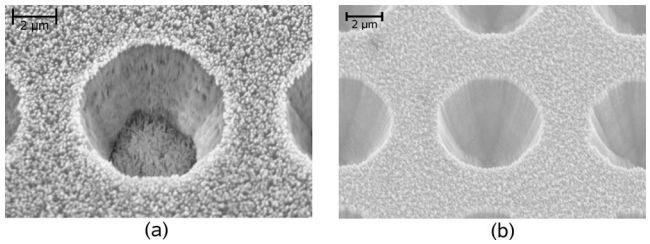


FIG. 5. SEM photographs of etched lithium niobate using an electroplated nickel layer as the etching mask. The diameter of the holes is 6 $\mu$m. The operating pressure was 0.2 Pa in both cases while the rf power was set to 250 W in (a) and 200 W in (b).

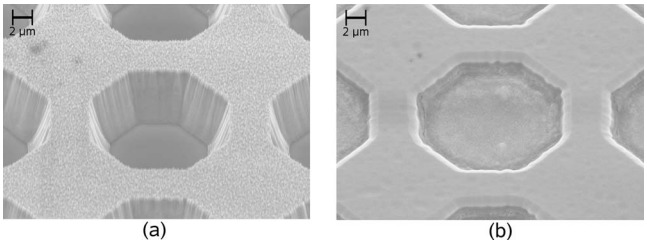


FIG. 6. SEM photographs of etched lithium niobate using an electroplated nickel layer as the etching mask. The diameter of the holes is 14 $\mu$m. A 200 W rf power was applied in both cases while the pressure was equal to 0.2 Pa in (a) and 6 Pa in (b).

what was previously reported in the literature, that lithium niobate is more efficiently etched using a rather mechanical process. It has indeed been observed that the etch rates decreases when the applied pressure increases, showing that ion bombardment is predominant over chemical etching on this material. The etch rates in a RIE process indeed result from a combination of chemical etching and ion-assisted (mechanical) etching. As a general rule, an increase in pressure leads to a rise of the amount of ionized chemical species in the plasma, which should result in an enhancement of the chemical etch rate. Conversely, it leads to a decrease in the bias voltage. The ion electrostatic attraction toward the substrate is then reduced, which leads to a decrease in the ion energy, hence reducing the ion bombardment. Figure 7 shows that both sidewall slope angle and etch rate follow a trend defined by the bias voltage which is directly related to the applied power-pressure couple and which is an indirect measurement of the strength of the ion bombardment. This does not necessarily mean that better results could be achieved only by increasing the rf power even further, as material damage is likely to occur, as was shown in Fig. 5(a).

Electroplated nickel follows an opposite trend: an increase in the chemical contribution of the process ends up being detrimental to the mask selectivity as shown in Table II. Electroplated nickel masks were proven to exhibit a much higher selectivity than their sputtered metal or photoresist counterparts. Let us here mention that resist degradation during the etching process could be reduced through

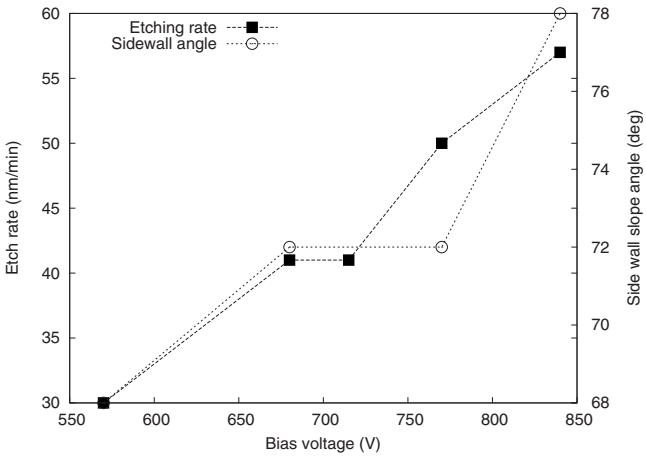


FIG. 7. Evolution of the etch rate and of the sidewall slope angle as a function of the bias voltage.

back side cooling of the sample which could help improving slightly the resist selectivity with respect to lithium niobate, without in any case allowing for high aspect ratio etching of the latter. The difference in selectivity observed between sputtered and electroplated nickel is probably due to the significant difference in crystalline morphology (size of the columns, roughness, density, Young's modulus, etc.), directly linked to the layer growth process parameters. It can be worth investigating the influence of these parameters (in particular, the influence of the current density) on the electroplated layer physical properties to try to relate them to the layer resilience to etching.

The surface of the substrate and at the bottom of the holes is as smooth as the unetched $LiNbO_3$ substrate, which is critical to ensure the propagation of surface acoustic waves, but the sidewall surface roughness is obviously highly dependent on the initial Ni mask contour shape. Electroplating allows to get rid of the defects usually observed in a lift-off process. Nevertheless, the rough columns constituting the material are directly transferred to the sidewalls. This can be of significance when aiming at fabricating ridge waveguides, for instance. It is, however, possible to change the electroplating parameters to grow metal layers exhibiting thinner columns. The influence on the selectivity, however, has to be investigated.

The presented process could also be improved by using the determined parameters as a basis for an ICP-RIE process. In an ICP system, two rf units allow controlling independently the ion density and the ion energy which allows bringing the plasma and density control a step further. This increase in plasma density generally result in better anisotropic etching capability compared to standard RIE along with higher etch rates and lower roughness, whatever the material. It is hence a more interesting alternative than imposing a sheer increase in the applied rf power in a standard capacitive system like a usual RIE machine. The idea would then be to enhance both lithium niobate etch rate and sidewall verticality while preserving the mask selectivity and the surface roughness of the process reported in the present paper.

Therefore, from the results presented in the previous sections, we eventually chose a process making use of a 1 $\mu$m thick electroplated nickel mask with the following RIE parameters: gas flow of 10 SCCM, operating pressure of 0.2 Pa, rf power of 200 W, and hence bias voltage around 750 V. The etch rate has been measured to be around 50 nm $min^{-1}$, the selectivity of electroplated Ni with respect to lithium niobate is about 20. If the mask selectivity does not limit the process in terms of achievable depth, the aspect ratio is limited to values around 1.5 by the sidewall slope angle. This latter cannot be attributed to the initial Ni mask as the mask verticality has been checked through SEM imaging, but is directly linked to the process itself. The developed process has been successfully applied to the fabrication of periodical arrays of octogons with a diameter of 9 $\mu$m and an interhole spacing of 900 nm on Y-cut, Y-128-cut lithium niobate substrates, without any noticeable difference. Similar results have been obtained on *Z*-axis oriented substrates. Figure 8(a) shows a SEM image of one of these structures. The hole array exhibits $10 \times 40$ holes. Here, the free surface of lithium

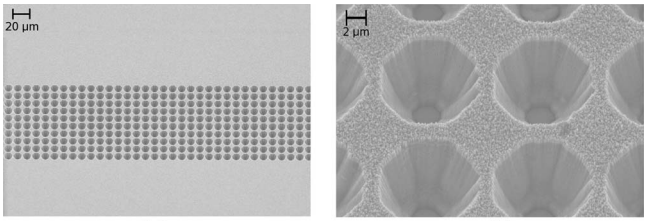


FIG. 8. SEM photograph of a phononic crystal structure etched in lithium niobate with a *Y*-axis crystallographic orientation at a rf power of 200 W and a pressure of 0.2 Pa. The period of the array is 10 $\mu$m, the hole diameter is 9.2 $\mu$m, and the hole depth is 10.5 $\mu$m. (b) Detail.

niobate is visible and the optical polish of the blank substrate was preserved by the electroplated mask. Figure 8(b) is a more detailed view taken straight after etching, before removal of the Ni mask. This latter is still visible and the remaining thickness has been evaluated to be around 500 nm. The $LiNbO_3$ etched depth is 10.5 $\mu$m and the sidewall slope angle is around 73°. This particular sample was subsequently used as a basis for the realization of phononic crystal devices for surface acoustic waves. A structure exhibiting a full band gap for SAW at a frequency around 200 MHz was hence demonstrated. The phononic crystal characterizations are fully reported elsewhere and are not reproduced here.[23,24]

## V. CONCLUSION

A process allowing for dry etching several micron-sized structures in lithium niobate using RIE was demonstrated. The etching process is based on a sulfur hexafluoride based chemistry at low pressure (0.2 Pa) and high rf power (200 W). The method involves using electroplated nickel as an etching mask, as this particular material presents a selectivity of the order of 20 with lithium niobate. Hole depth larger than 10 $\mu$m could be obtained, corresponding to sidewall slope angles as high as 73° while keeping a very good surface roughness. This process is perfectly relevant for the realization of structures with dimensions larger than 5 $\mu$m and aspect ratios typically around 1.5. Fabrication of microsonic phononic crystals or ridge waveguides is then possible. Further improvement is needed for the realization of high aspect ratio or submicron-sized structure such as phonic crystals, for instance. We are currently investigating the possibility to use ICP-RIE to enhance the obtained wall profiles.

## ACKNOWLEDGMENTS

The authors gratefully acknowledge Gwenn Ulliac for enlightening discussion, as well as Denis Bitschene for technical assistance.

[1]E. L. Wooten, K. M. Kissa, A. Yi-Yan, E. J. Murphy, D. A. Lafaw, P. F. Hallemeier, D. Maack, D. V. Attanasio, D. J. Fritz, G. J. McBrien, and D. E. Bossi, IEEE J. Sel. Top. Quantum Electron. **6**, 69 (2000).
[2]M. Roussey, M.-P. Bernal, and F. Baida, Appl. Phys. Lett. **87**, 241101 (2005).
[3]K. Nassau, H. J. Levinstein, and G. M. Loiacono, Appl. Phys. Lett. **6**, 228 (1965).
[4]I. E. Barry, G. W. Ross, P. G. R. Smith, R. W. Eason, and G. Cook, Mater. Lett. **37**, 246 (1998).
[5]F. Laurell, J. Webjorn, G. Arvidsson, and J. Holmberg, J. Lightwave Technol. **10**, 1606 (1992).
[6]I. P. Kaminow, V. Ramaswamy, R. V. Schmidt, and E. H. Turner, Appl. Phys. Lett. **24**, 622 (1974).
[7]M. Minakata, Appl. Phys. Lett. **35**, 40 (1979).
[8]S. Yin, Microwave Opt. Technol. Lett. **22**, 396 (1999).
[9]F. Lacour, N. Courjal, M.-P. Bernal, A. Sabac, C. Bainier, and M. Spajer, Opt. Mater. (Amsterdam, Neth.) **27**, 1421 (2005).
[10]C. I. H. Ashby and P. J. Brannon, Appl. Phys. Lett. **49**, 475 (1986).
[11]P. T. Brown, S. Mailis, I. Zergiotti, and R. W. Eason, Opt. Mater. (Amsterdam, Neth.) **20**, 125 (2002).
[12]F. K. Christensen and M. Müllenborn, Appl. Phys. Lett. **66**, 2772 (1995).
[13]W. Yang, H. Lee, W. Kim, and D. Yoon, Opt. Mater. (Amsterdam, Neth.) **27**, 1642 (2005).
[14]C. L. Lee and C. L. Lu, Appl. Phys. Lett. **35**, 756 (1979).
[15]J. L. Jackel, R. E. Howard, E. L. Hu, and S. P. Lyman, Appl. Phys. Lett. **38**, 907 (1981).
[16]V. Foglietti, E. Cianci, D. Pezzetta, C. Sibiliab, M. Marangonic, R. Osellamec, and C. R. Ramponi, Microelectron. Eng. **67–68**, 742 (2003).
[17]W. J. Park, W. S. Yang, W. K. Kim, H. Y. Lee, J. W. Lim, M. Isshiki, and D. H. Yoon, Opt. Mater. (Amsterdam, Neth.) **28**, 216 (2006).
[18]H. Hu, A. P. Milenin, R. B. Wehrspohn, H. Hermann, and W. Sohler, J. Vac. Sci. Technol. A **24**, 1012 (2006).
[19]Z. Ren, P. J. Heard, J. M. Marshall, P. A. Thomas, and S. Yu, J. Appl. Phys. **103**, 034109 (2008).
[20]G. Ulliac, N. Courjal, H. M. H. Chong, and R. M. De La Rue, Opt. Mater. (Amsterdam, Neth.) **31**, 196 (2008).
[21]H. Nagata, N. Mitsugi, K. Shima, M. Tamai, and E. M. Haga, J. Cryst. Growth **187**, 573 (1998).
[22]V. Laude, M. Wilm, S. Benchabane, and A. Khelif, Phys. Rev. E **71**, 036607 (2005).
[23]S. Benchabane, A. Khelif, J.-Y. Rauch, L. Robert, and V. Laude, Phys. Rev. E **73**, 065601(R) (2006).
[24]K. Kokkonen, M. Kaivola, S. Benchabane, A. Khelif, and V. Laude, Appl. Phys. Lett. **91**, 083517 (2007).